Full quantum-mechanical study of protonium formation in slow collisions of antiprotons with hydrogen atoms

Kazuhiro Sakimoto*
Institute of Space and Astronautical Science, Yoshinodai, Sagamihara 229-8510, Japan
(Received 8 July 2001; published 12 December 2001)

A rigorous full quantum-mechanical wave-packet calculation is carried out to study the protonium formation $\bar{p}+\mathrm{H}\rightarrow\bar{p}p+e$. The present paper directly solves the time-dependent Schrödinger equation for the heavy particle Coulomb collision system. A discrete-variable-representation technique is used to evaluate the action of the Hamiltonian operator on the wave packet. The cross sections for the protonium formation are obtained at center-of-mass translational energies up to 10 eV. The present quantum-mechanical results are compared with those of previous studies based on classical trajectory Monte Carlo and semiclassical methods. Applicability of the adiabatic molecular picture to the protonium formation is also discussed.

DOI: 10.1103/PhysRevA.65.012706 PACS number(s): 34.50.Fa, 36.10.−k, 34.50.Lf

I. INTRODUCTION

In the antiproton decelerator facility at CERN, low-energy antiprotons ($\bar{p}$) are now experimentally available for various purposes [1,2]. The study of the interaction between antiprotons and ordinary matters is of special importance to test fundamental physical principles such as charge-parity-time invariance and the gravitational weak equivalence principle. Projects for such experimental studies are progressing as the collaborations of ASACUSA, ATHENA, and ATRAP [1,2]. As the need arises, the collision processes involving antiprotons become very important also from the point of view of atomic physics.

The collision of antiprotons with hydrogen atoms may be regarded as one of the most basic processes in atomic physics, and is interesting also as a production process of protonium atoms ($\bar{p}p$). Since the collision is a three-body problem, its rigorous numerical treatment is possible by the use of recent computers. In the present study, we carry out a rigorous full quantum-mechanical (QM) calculation to obtain the cross section for the protonium formation

$$\bar{p}+\mathrm{H}(1s)\rightarrow\bar{p}p+e. \tag{1.1}$$

This rearrangement process becomes important only at energies less than about the threshold of breakup ionization ($\bar{p}+p+e$) [3–6]. We consider the center-of-mass translational energies up to 10 eV. In this energy region, the breakup ionization channel is closed, and thereby the emission of electrons just means the formation of protonium atoms.

So far, several theoretical studies have been made for the protonium formation (1.1). Cohen [3–5] and Schultz *et al.* [6] applied a classical trajectory Monte Carlo (CTMC) method. However, a classical treatment would not be appropriate to describe the low-energy collisions and especially the electron motion. Cohen [4,5] also took partly account of a QM effect in the CTMC calculation by means of a momentum-dependent pseudopotential, which had been first introduced by Kirschbaum and Wilets [7] for the study of atomic structure. As another way, an adiabatic molecular (i.e., quantum chemistry) picture may be applicable because the process (1.1) occurs at low energies. The QM nature of the electron motion during the collision may be able to be implicitly taken into account in the adiabatic potential. By supposing that the classical trajectory of the relative motion is determined from the adiabatic potential, Morgan and Hughes [8,9] estimated the adiabatic limit of the cross section for the protonium formation (1.1). Very recently, the present author [10] (hereafter referred to as paper I) has shown that the nonadiabatic transition is rather a dominant mechanism for the formation process (1.1). In the adiabatic picture, the electron emission cannot occur unless the relative radial distance R between $\bar{p}$ and H becomes less than the so-called Fermi-Teller radius $R_{\mathrm{FT}}=0.639$ a.u. (c.f., Fig. 1). On the contrary, paper I has shown that the probability for the protonium formation still remains unity even if the closest distance is larger than R_{FT}; the formation probability falls off from unity when the closest distance is $R>1$ a.u., and becomes negligibly small at last for $R>2$ a.u. For this reason, if we rely on the adiabatic picture, the formation cross section is underestimated in the energy region above 1 eV [10]. As a full QM study, Voronin and Carbonell [11] have carried out a calculation for the process (1.1) by introducing a coupled-channel model, in which the effect of closed channels corresponding to the protonium continuum states is presumed to be the appearance of the polarization potential. Only the s and p waves have been calculated for the total angular momentum, and accordingly, they have studied the low-energy limit ($<10^{-4}$ eV) of the formation cross section. As shown in CTMC studies [4,5] and in paper I, the total angular momentum quantum numbers up to ~ 50 contribute to the formation cross section at energies $\lesssim 10$ eV.

In paper I, the present author has studied the formation process (1.1) within a framework of a semiclassical (SC) theory. A SC approach was also made for the negative muon (μ^-) capture, i.e., $\mu^-+\mathrm{H}\rightarrow\mu^- p+e$ [12]. In these SC treat-

*Email address: sakimoto@pub.isas.ac.jp

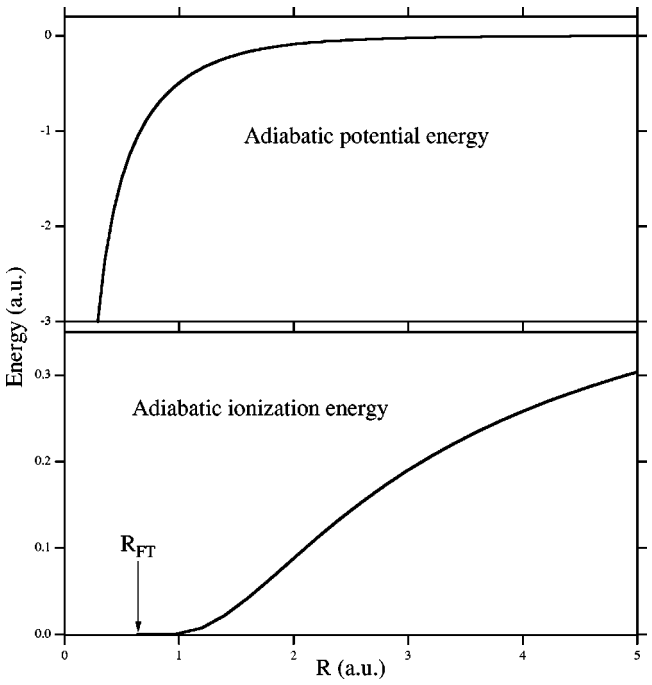

FIG. 1. Adiabatic potential and adiabatic ionization energies of the $\bar{p}$+H system, taken from Walls *et al.* [20]. The ionization energy vanishes at the Fermi-Teller radius $R_{FT}=0.639$ a.u., and becomes 0.5 a.u. as $R\rightarrow\infty$.

ments, a common classical trajectory is assumed for the relative motion between a massive negative particle and a hydrogen atom, and the other motions are described in quantum mechanics. In paper I, the common trajectory is defined in the way that the expectation of the total Hamiltonian is equal to the total energy (i.e., the energy conservation in an average sense). Although this assumption seems to be one of the most appropriate choices, there is no unambiguous way to define a common trajectory in a semiclassical manner. Furthermore, it is not certain that the common trajectory treatment is satisfactory to describe the rearrangement process such as Eq. (1.1) at low energies. Carrying out a full QM calculation is necessary to precisely understand the collision dynamics.

In paper I, the variable treated in classical mechanics is only one degree of freedom, i.e., the relative radial distance R, and the conservation of the total angular momentum is already taken into account. Therefore, we can straightforwardly extend the calculation of paper I to the full QM manner though the numerical computation becomes substantially laborious. As the natural extension of paper I, we adopt a time-dependent wave-packet propagation picture to describe the collision process. In paper I, a numerical technique of discrete variable representation (DVR) [13] has been used to solve the time-dependent Schrödinger equation. The efficiency of the DVR technique for the $\bar{p}$+H collision has been already discussed elsewhere [14,15]. The present work is an attempt to apply the time-dependent full QM method to heavy particle collisions of the Coulomb three-body system by using the DVR numerical technique.

II. THEORY AND NUMERICAL METHOD

A. Total Hamiltonian operator

In the three-body system, three sets of Jacobi coordinates each correspond to different arrangement channels. Here, we describe the collision process (1.1) in the Jacobi coordinates suitable for the $\bar{p}+ep$ arrangement: namely, **R** and **r** denote the position vectors of $\bar{p}$ from the center-of-mass of H and of e from p, respectively. The related reduced masses μ and m are expressed in terms of the electron mass m_e and the proton (antiproton) mass m_p as

$$\mu=\frac{m_p(m_e+m_p)}{m_e+2m_p},\quad m=\frac{m_e m_p}{m_e+m_p}. \tag{2.1}$$

Since the calculation is carried out merely for the total probability for the protonium formation in the present study, as seen later, we may do without the other sets of Jacobi coordinates. (A summary of the Jacobi coordinates for the $e+\bar{p}p$ channel is shown in the Appendix.)

We further employ a body-fixed (BF) frame in which the z axis is chosen along **R**. The rotation from a space-fixed (SF) frame to the BF frame is represented by the Euler angles (α,β,γ), where $\hat{\mathbf{R}}=(\beta,\alpha)$ in the SF frame and γ is the azimuthal angle of $\hat{\mathbf{r}}$. Then, the total Hamiltonian operator of the three-body system may be written as [16,17]

$$\tilde{H}=-\frac{1}{2\mu R}\frac{\partial^2}{\partial R^2}R+\frac{(\tilde{\mathbf{L}}-\tilde{\mathbf{l}})^2}{2\mu R^2}-\frac{1}{2mr}\frac{\partial^2}{\partial r^2}r+\frac{\tilde{\mathbf{l}}^2}{2mr^2}+V(R,r,\theta), \tag{2.2}$$

where θ is the polar angle of $\hat{\mathbf{r}}$. We use atomic units unless otherwise stated. In Eq. (2.2), $\tilde{\mathbf{L}}$ and $\tilde{\mathbf{l}}$ are the total and electronic angular momentum vectors (operators), respectively,

$$(\tilde{\mathbf{L}}-\tilde{\mathbf{l}})^2=\tilde{\mathbf{L}}^2+\tilde{\mathbf{l}}^2-2\tilde{L}_z\tilde{l}_z-\tilde{l}_+\tilde{L}_--\tilde{l}_-\tilde{L}_+ \tag{2.3}$$

is the Coriolis operator [18], and $V(R,r,\theta)$ is the sum of all the Coulomb potentials, i.e.,

$$V=\left|\mathbf{R}-\frac{m_p}{m_e+m_p}\mathbf{r}\right|^{-1}-\left|\mathbf{R}+\frac{m_e}{m_e+m_p}\mathbf{r}\right|^{-1}-r^{-1}. \tag{2.4}$$

B. Time-dependent Schrödinger equation

The time-dependent picture is employed to solve the collision problem. The time-dependent Schrödinger equation for the total wave function Ψ^{LM} is

$$i\frac{\partial}{\partial t}\Psi^{LM}(\mathbf{R},\mathbf{r},t)=\tilde{H}\Psi^{LM}(\mathbf{R},\mathbf{r},t), \tag{2.5}$$

where L and M are the total angular momentum quantum number and its magnetic component in the SF frame, respectively. The total wave function Ψ^{LM} may be written in the form [14]

$$\Psi^{LM}(\mathbf{R},\mathbf{r},t)=(Rr)^{-1}\sum_{\lambda}\ \bar{D}^{L}_{M\lambda}(\alpha,\beta,\gamma)\psi^{L\lambda}(R,r,\theta,t), \tag{2.6}$$

where

$$\bar{D}^{L}_{M\lambda}(\alpha,\beta,\gamma)=\left[\frac{2L+1}{8\pi^2}\right]^{1/2}[D^{L}_{M\lambda}(\alpha,\beta,\gamma)]^{*} \tag{2.7}$$

is the normalized Wigner's rotation matrix element [19], and $\lambda=\tilde{L}_z=\tilde{l}_z$ is the magnetic quantum number in the BF frame. In the actual calculation, the conservation of parity is further take into account [14] though it is not shown explicitly here. The time-dependent wave function (2.6) has the same form as the semiclassical one given in paper I except for the radial R part.

We may write the stationary solution of Eq. (2.5) in the form

$$\Psi^{LM}(\mathbf{R},\mathbf{r},E)\exp(-\mathrm{i}Et), \tag{2.8}$$

where $\Psi^{LM}(E)$ is the time-independent wave function for the total energy E, i.e.,

$$(\tilde{H}-E)\Psi^{LM}(\mathbf{R},\mathbf{r},E)=0, \tag{2.9}$$

and is given by [16,17]

$$\Psi^{LM}(\mathbf{R},\mathbf{r},E)=(Rr)^{-1}\sum_{\lambda}\ \bar{D}^{L}_{M\lambda}(\alpha,\beta,\gamma)\psi^{L\lambda}(R,r,\theta,E). \tag{2.10}$$

In terms of the time-independent wave function $\psi^{L\lambda}(E)$ in Eq. (2.10), the time-dependent (nonstationary) solution $\psi^{L\lambda}(t)$ in Eq. (2.6) may be expanded as the wave packet having the form

$$\psi^{L\lambda}(R,r,\theta,t)=\int\ C(E)\psi^{L\lambda}(R,r,\theta,E)\exp(-\mathrm{i}Et)dE. \tag{2.11}$$

The coefficient $C(E)$ determines an explicit form of the initial wave packet $\psi^{L\lambda}(t=0)$, and is normalized to unity,

$$\int\ |C(E)|^2dE=1. \tag{2.12}$$

Evidently, the quantity $|C(E)|^2$ gives the energy distribution of the initial wave packet.

C. Asymptotic form of time-independent wave function

To calculate the S-matrix elements for collisional transition, we see the asymptotic form of the time-independent wave function $\psi^{L\lambda}(E)$. Because of the low-energy collision, the adiabatic state may be used to define the asymptotic channels. As shown in paper I, the use of the adiabatic basis leads to the reduction of the computation time. The adiabatic basis is given by the following eigenvalue equation for each fixed R:

$$\left[-\frac{1}{2m}\frac{\partial^2}{\partial r^2}+\frac{\tilde{\mathbf{l}}^2}{2mr^2}+V(R,r,\theta)\right]\chi_{\Gamma\lambda}(r,\theta;R)$$
$$=E_{\Gamma\lambda}(R)\ \ \chi_{\Gamma\lambda}(r,\theta;R), \tag{2.13}$$

where (Γ,λ) classifies the adiabatic state. In Fig. 1, the adiabatic potential $E_{\Gamma\lambda}(R)-E_{\Gamma\lambda}(R\to\infty)$ and the adiabatic ionization energy, taken from Walls *et al.* [20], are shown for the electronic ground state. [The adiabatic states of Walls *et al.* are given by setting $m_p\to\infty$ in Eq. (2.13), but the difference is actually negligible.] In the $\bar{p}+\mathrm{H}$ system, the adiabatic state is meaningless at $R\leqslant R_{\mathrm{FT}}$ because the electronic bound states are absent. When $R>2$ a.u., the nonadiabatic coupling becomes negligible [14,10]. Accordingly, for sufficiently large $R(\gg 2$ a.u.), the wave function may be written in the form

$$\psi^{L\lambda}(R,r,\theta,E)=\chi_{\Gamma_0\lambda_0}(r,\theta;R)f^{-}_{\Gamma_0\lambda_0}(R)\delta_{\lambda\lambda_0}$$
$$-\sum_{\Gamma}\ \chi_{\Gamma\lambda}(r,\theta;R)\ \ f^{+}_{\Gamma\lambda}(R)S^{L}_{\Gamma\lambda,\Gamma_0\lambda_0}, \tag{2.14}$$

where $S^{L}_{\Gamma\lambda,\Gamma_0\lambda_0}$ is the S-matrix element for the elastic (or inelastic) transition. The breakup ionization channel is closed in the present energy region. To take account of the R dependences of the centrifugal potential and the adiabatic basis, the WKB functions are used to express the incoming $(-)$ and outgoing $(+)$ waves [21]:

$$f^{\pm}_{\Gamma\lambda}(R)=\left[\frac{\mu}{2\pi k_{\Gamma\lambda}(R)}\right]^{1/2}\exp\left[\pm\mathrm{i}\int^{R}k_{\Gamma\lambda}(R')dR'\right] \tag{2.15}$$

with the local radial wave-number $k_{\Gamma\lambda}(R)$ defined by

$$k_{\Gamma\lambda}(R)=\left\{2\mu\left[E-\frac{L(L+1)-2\lambda^2}{2\mu R^2}-E_{\Gamma\lambda}(R)\right]\right\}^{1/2}. \tag{2.16}$$

In the Appendix, we present the asymptotic form of the time-independent wave function representing the $e+\bar{p}p$ channel. This asymptotic form becomes essential only if we intend to calculate the final-state specified probabilities for the protonium formation. However, the consideration of the asymptotic form (2.14) alone is sufficient just for the calculation of the formation probability summed over all the final states.

D. Preparation of initial wave packet

The initial condition of $\psi^{L\lambda}(t)$ at $t=0$ may be taken as

$$\psi^{L\lambda}(R,r,\theta,t=0)=\chi_{\Gamma_0\lambda_0}(r,\theta;R)\zeta(R)\delta_{\lambda\lambda_0}. \tag{2.17}$$

Here, (Γ_0,λ_0) is the initial state of the hydrogen atom, and a Gaussian wave packet is assumed for $\zeta(R)$, i.e.,

$$\zeta(R)=(2\pi\delta^2)^{-1/4}\exp\left[-\frac{(R-R_0)^2}{4\delta^2}-\mathrm{i}\,k_0(R-R_0)\right], \tag{2.18}$$

where δ is a width parameter, R_0 is the center of the wave packet, and k_0 is the center in the momentum space. From Eqs. (2.14) and (2.17), the coefficient $C(E)$ in Eq. (2.11) may be given by

$$C(E)=\langle f^-|\zeta\rangle. \tag{2.19}$$

When R is large, the adiabatic wave-function $\chi_{\Gamma_0\lambda_0}(r,\theta;R)$ is loosely dependent on R. Therefore, if the wave-packet $\zeta(R)$ is well localized around R_0, we may assume $\chi_{\Gamma_0\lambda_0}(r,\theta;R)=\chi_{\Gamma_0\lambda_0}(r,\theta;R_0)$ in the initial condition (2.17). However, the R dependence of the local wave-number $k_{\Gamma\lambda}(R)$ should not be neglected in the calculation of Eq. (2.19).

E. Analysis of final wave packet

To extract the S-matrix elements or the transition probabilities from the scattered wave packet, we need to make a proper analysis of the wave packet. This is done in the following way. We introduce a fixed radial distance $R=R_\mathrm{f}$ where the asymptotic form (2.14) is satisfied. Making a time integral (Fourier transform) at $R=R_\mathrm{f}$, we define the energy-dependent amplitude:

$$A^L_{\Gamma\lambda,\Gamma_0\lambda_0}(E)=\frac{1}{\sqrt{2\pi}}\int_{t_0}^{\infty}\exp(\mathrm{i}Et)\langle\chi_{\Gamma\lambda}|\psi^{L\lambda}(t)\rangle_{R=R_\mathrm{f}}dt, \tag{2.20}$$

where t_0 is the first time that satisfies $\psi^{L\lambda}(t_0)=0$ at $R=R_\mathrm{f}$ just after the incoming phase of the wave-packet propagation. If the S-matrix elements are requested for a center-of-mass translational energy E_t, the total energy E is give as

$$E=E_\mathrm{t}-I_{\Gamma_0\lambda_0}, \tag{2.21}$$

where $I_{\Gamma_0\lambda_0}=-E_{\Gamma_0\lambda_0}(R\to\infty)$ is the ionization energy of the hydrogen atom. From Eqs.(2.11), (2.14), and (2.20), we can easily show that

$$S^L_{\Gamma\lambda,\Gamma_0\lambda_0}(E)=-\frac{A^L_{\Gamma\lambda,\Gamma_0\lambda_0}(E)}{\sqrt{2\pi}C(E)f^+_{\Gamma\lambda}(R_\mathrm{f})}. \tag{2.22}$$

Alternatively, using the flux formalism, a numerically more convenient expression for the transition probability $P^L_{\Gamma\lambda,\Gamma_0\lambda_0}=|S^L_{\Gamma\lambda,\Gamma_0\lambda_0}|^2$ is directly given by [22,23]

$$P^L_{\Gamma\lambda,\Gamma_0\lambda_0}(E)=\frac{1}{\mu|C(E)|^2}\mathrm{Im}\left[(A^L_{\Gamma\lambda,\Gamma_0\lambda_0})^*\frac{dA^L_{\Gamma\lambda,\Gamma_0\lambda_0}}{dR_\mathrm{f}}\right]. \tag{2.23}$$

Since the breakup ionization channel is closed here, the probability for the protonium formation may be calculated from

$$P^L_{\bar{p}p}(\Gamma_0\lambda_0)=1-\sum_{\Gamma\lambda}P^L_{\Gamma\lambda,\Gamma_0\lambda_0}, \tag{2.24}$$

where the sum is taken over all the bound states of the hydrogen atom. Finally, the formation cross section is defined by

$$\sigma^-_{\bar{p}p}(\Gamma_0\lambda_0)=\frac{\pi}{[k_{\Gamma_0\lambda_0}(R\to\infty)]^2}\sum_L(2L+1)P^L_{\bar{p}p}(\Gamma_0\lambda_0). \tag{2.25}$$

F. Discrete variable representation

In solving the time-dependent Eq. (2.5), we use the DVR technique [13] to evaluate the action of the Hamiltonian operator on the wave packet. In the DVR method, a grid is constructed from zero points of an orthogonal polynomial. We introduce a grid-based function $u_n(x)$ [24]

$$u_n(x)=[\omega_n W(x)]^{1/2}\sum_\tau^N F_\tau(x_n)F_\tau(x), \tag{2.26}$$

where $F_\tau(x)$ is a normalized orthogonal polynomial of degree τ; and x_n is the zero point of $F_N(x)$; $W(x)$ is the weight function; and ω_n is the quadrature weight. Arbitrary types of orthogonal polynomials are acceptable. The grid-based function satisfies the following orthogonal properties:

$$u_n(x_{n'})=\left(\frac{W_n}{\omega_n}\right)^{1/2}\delta_{nn'},\quad \langle u_n|u_{n'}\rangle=\delta_{nn'}, \tag{2.27}$$

where we have put $W_n=W(x_n)$.

As shown recently in Ref. [15], the (generalized) Laguerre polynomials [25]

$$F_\tau(r)=[(\tau+2)(\tau+1)]^{-1/2}L^{(2)}_\tau(r) \tag{2.28}$$

are appropriate for the r coordinate because of the Coulomb nature. One may expect that the Legendre polynomials

$$F_\tau(\cos\theta)=(2\tau+1)^{1/2}P_\tau(\cos\theta) \tag{2.29}$$

are efficient for the θ coordinate. However, this is true only when $\lambda=$ even [27,26]. The present author [26] has shown that the following ultraspherical (or Jacobi) polynomials [25]

$$F_\tau(\cos\theta)=\left[\frac{(2\tau+1)(\tau+1)}{4\tau}\right]^{1/2}P^{(1,1)}_{\tau-1}(\cos\theta) \tag{2.30}$$

should be used in the case of odd λ. For the R coordinate, we use the Chebyshev polynomials

$$F_\tau\left(\sin\frac{\pi R}{R_\mathrm{max}}\right)=\sqrt{\frac{2}{\pi}}\sin\frac{\tau\pi R}{R_\mathrm{max}}, \tag{2.31}$$

where $R_{\max}$ defines the outermost radius in the numerical calculation. It is mentioned that only the Chebyshev zero points construct an equally spaced grid.

Putting $u_i(\pi R/R_{\max})$, $u_j(r)$, and $u_k^{\lambda=\text{even/odd}}(\cos\theta)$ as the DVR functions (2.26) for the coordinates R, r, and θ, respectively, we may have

$$\psi^{L\lambda}(R,r,\theta,t)=\sum_{ijk}\left(\frac{\omega_i\omega_j\omega_k^{\lambda}}{W_iW_jW_k^{\lambda}}\right)^{1/2}\psi^{L\lambda}(R_i,r_j,\theta_k^{\lambda},t)\times u_i(\pi R/R_{\max})u_j(r)u_k^{\lambda}(\cos\theta), \quad (2.32)$$

where $W_i=1$, $W_j=r_j^2e^{-r_j}$, $W_k^{\lambda=\text{even}}=1$, $W_k^{\lambda=\text{odd}}=\sin^2\theta_k^{\lambda=\text{odd}}$; and ω_i, ω_j, $\omega_k^{\lambda=\text{even}}$, and $\omega_k^{\lambda=\text{odd}}$ are the quadrature weights of the Chebyshev, Laguerre, Legendre, and ultraspherical polynomials, respectively. Inserting Eq. (2.32) into the time-dependent Schrödinger Eq. (2.5), and using the orthogonalities (2.27), we have a set of coupled linear equations with respect to the wave packet given on the DVR grid points $(R_i,r_j,\theta_k^{\lambda})$, i.e.,

$$\frac{d\psi_{ijk}^{L\lambda}(t)}{dt}=\sum_{\lambda'i'j'k'}[M_{ijk,i'j'k'}^{\lambda,\lambda'}-iV(R_i,r_j,\theta_k^{\lambda})\delta_{\lambda\lambda'}\delta_{ii'}\delta_{jj'}\delta_{kk'}]\psi_{i'j'k'}^{L\lambda'}(t), \quad (2.33)$$

where we have put

$$\psi_{ijk}^{L\lambda}(t)=\left(\frac{\omega_i\omega_j\omega_k^{\lambda}}{W_iW_jW_k^{\lambda}}\right)^{1/2}\psi^{L\lambda}(R_i,r_j,\theta_k^{\lambda},t). \quad (2.34)$$

The coupling matrix elements $M_{ijk,i'j'k'}^{\lambda,\lambda'}$ come from only the kinetic-energy operators, and hence, this matrix is sparse. This is a great advantage of the DVR method in the numerical computation. The explicit forms of $M_{ijk,i'j'k'}^{\lambda,\lambda'}$ are easily calculated using the properties of orthogonal polynomials [24], and can be found in previous papers [14,15].

G. Numerical calculations

We have prepared the initial wave-packet (2.17) by taking $\delta=0.25$ a.u. and $R_0=4$ a.u., and have set $R_f=R_0$. The hydrogen atom is assumed to be initially in the ground $1s$ state. Since the energy range of $E_t\leqslant 10$ eV is considered, the elastic $[\bar{p}+\mathrm{H}(1s)]$ and protonium formation channels are open in the collision, and the other inelastic $[\bar{p}+\mathrm{H}(n\geqslant 2)]$ and breakup ionization channels are closed. The value of $R_0=4$ a.u. is slightly smaller than the initial distance ($R=5$ a.u.) chosen in paper I. We have confirmed the appropriateness of this choice by comparing with the results for $R_0=R_f=6$ a.u. When we make the integral (2.20) over a long time, the portions of the wave packet propagated backward into the entrance channel will eventually reach the edge of the grid $R=R_{\max}$, and will be reflected back onto the grid. This phenomena is evidently unphysical, and produces a fictitious result in the present calculation. The choice of a sufficiently large value of $R_{\max}$ resolves the edge problem, but makes the computation time impractical. As usually done in most of the wave-packet propagation calculations [28], we have applied a negative imaginary (absorbing) potential [29] near the edge, and thereby we can choose $R_{\max}=6$ a.u.

The central translational energies $E_t^0=k_0^2/2\mu$ of the initial Gaussian wave packet (2.18) have been taken to be 5 and 7.5 eV for the calculation of the formation cross sections. The wave packet has some range of translational energies E_t. The weight of each energy component is given by Eq. (2.19). In the present study, the probability has been extracted for the translational energy E_t that satisfies

$$\left|\frac{C(E_t-I_{1s})}{C(E_t^0-I_{1s})}\right|^2>0.1. \quad (2.35)$$

Then, the two wave packets of $E_t^0=5$ and 7.5 eV cover the energy range of $3\lesssim E_t\lesssim 10$ eV. We have checked the accuracy of this extraction by taking $E_t^0=E_t$ for the initial wave packet, and we estimate that the error of the formation probabilities in the present calculation is much less than 1%. As the occasion demands, another value has been chosen for the central energy E_t^0.

The number of grid points has been changed according to the total angular momentum L. We have taken $N_R=60$–200 (a larger value of N_R for low L where the wave packet reaches small R) and $N_r=20$–40 (a larger value of N_r for high L where the formation probability becomes small). In the process (1.1), the protonium is formed in very high orbital states. The present choice for N_R gives, for example, the protonium energies of -7.8203 eV for the angular momentum $\bar{l}=10$, -7.8128 eV for $\bar{l}=20$, and -7.8126 eV for $\bar{l}=30$ when the principal quantum number $\bar{n}$ is 40, while the accurate value is -7.8126 eV. A convergence check for the description of the hydrogen bound states has been given in Ref. [15]. Voronin and Carbonell [11] found that the consideration of the electronic angular momenta $l=0$ and 1 were sufficient in their calculation because of the very light mass of an electron. In the present calculation, the value of $N_\theta=2$ or 3 has been chosen, and the states with $\lambda=0$ and 1 have been coupled. This consideration for the angular part corresponds to the inclusion of the electronic angular momenta up to $l=3$ or 4. All these choices have been made so that the convergence error of the cross sections is estimated to be less than a few percent. To solve the time-dependent linear Eqs. (2.33), a fourth-order Runge-Kutta formula has been applied although several numerically efficient methods were developed [28]. A simple method of the Runge-Kutta algorithm has sufficiently served the present purpose. For the matrix multiplication in the right-hand side of Eq. (2.33), the number of the numerical operations is not so tremendous since the coupling matrix is sparse and may be easily stored in advance. The calculation has not been made for all the partial waves required in the summation (2.25). Since the probabilities form a smooth function of L, those for partial waves not calculated may be obtained appropriately by a cubic-spline interpolation.

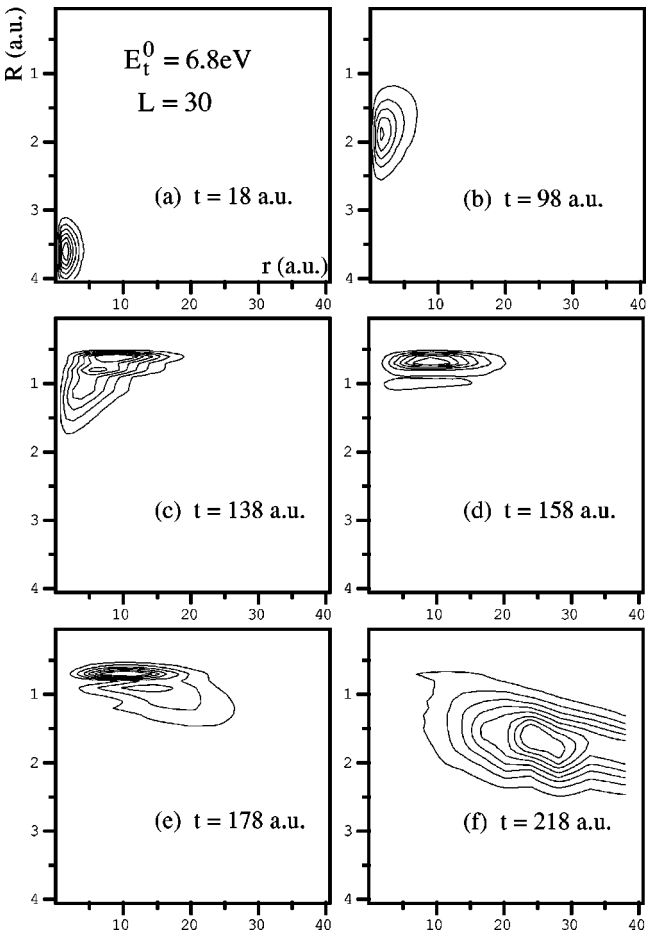

FIG. 2. Plots of the probability distribution $\rho^{L=30}(R,r,t)$ for $E_t^0=6.8$ eV at different points of time, as shown by contours.

In Ref. [15], we have found that the Laguerre grid is more attractive to describe the electron continuum motion than the Chebyshev grid since the argument of the Laguerre polynomials ranges to infinity. It should be noted, however, that the interval between adjacent grid points increases rapidly for very large r_j. (As an example, when $N_r=30$, the interval is about 4.5 a.u. for $r\sim 40$ a.u. The interval around the same r decreases with increasing N_r.) Therefore, the Laguerre grid is certainly not suitable for an accurate description of the electron continuum motion in the asymptotic region. The practical use of the Laguerre grid is limited to the electron motion in the range $r<r_{N_r}$. Furthermore, the reflection of the wave packet occurs unphysically around $r=r_{N_r}$. This reflection causes a problem when long-time propagation is required. Fortunately, here we do not need to know detailed information on the wave packet for large r since the final-state specified formation probabilities are not calculated. Therefore, a negative imaginary potential [29] has been applied also at $r>r_{\rm op}=40$ a.u. to avoid the above troublesome problems. However, owing to the sparseness of the Laguerre grid for large r_j, the imaginary potential has not been able to work absolutely for the absorption of the wave packet. The efficiency of the imaginary potential improves with increasing N_r. In the present choice of N_r, we have found that the function of the imaginary potential is efficient enough to make the reflection effect negligible at energies $E_t\gtrsim 3$ eV. To calculate the time integral (2.20) for these energies, we need the end time up to $t\sim 900$ a.u. If the translational energy is lower, longer-time propagation is required, and a larger value of N_r will be necessary.

III. RESULTS AND DISCUSSION

A. Time evolution

In Figs. 2 and 3, we show the time evolution of the probability distribution defined by

$$\rho^L(R,r,t)=R^2r^2\int |\Psi^{LM}(\mathbf{R},\mathbf{r},t)|^2 d\hat{\mathbf{R}}\,d\hat{\mathbf{r}}. \qquad (3.1)$$

The wave packets prepared for the figures are for the central translational energy $E_t^0=6.8$ eV and the total angular momenta $L=30$ and 40. The wave packet is initially localized around the position of $R=4$ a.u. and $r\simeq 1.5$ a.u., and is then propagated through the entrance channel (i.e., along the R axis). The panels (a) and (b) of the figures correspond to this early stage. The panels (c) or (d) indicate the dynamical feature that the wave packet is just reflected back along R by the centrifugal barrier. We see that the position (R) of the reflection area is an important factor to understand the formation mechanism. The protonium formation is expressed as two dynamical actions of the wave packet, i.e., the stretch of the wave packet along r and then the breakaway of its portions into large r. These two successive actions are rapid because they are also related to the escape motion of the electron, and are nearly completed while the wave packet is lying around the reflection area. The reflection position is mostly $R<1$ a.u. for the lower angular momentum $L=30$, and is $1<R<2$ a.u. for the higher $L=40$. When $L=30$, after the reflection, the most portions of the wave packet move through the $e+\overline{p}p$ channel (i.e., along the r axis), and never return into large R. This means that the protonium atom is formed in the probability of nearly unity. When $L=40$, on the other hand, the main part of the wave packet is propagated backward into the entrance channel, and the protonium formation does not occur so frequently. In the SC study of paper I, we have been able to see a similar dynamical aspect, which are characterized well in terms of the first turning point of the common trajectory.

In Fig. 4, the time evolution of the electron distribution defined by

$$\rho^L(r,t)=\int \rho^L(R,r,t)dR \qquad (3.2)$$

is shown for three total angular momenta at the central translational energy $E_t^0=7.5$ eV. The three partial waves of $L=30$, 40, and 50 represent the wave packets mostly moving through the $e+\overline{p}p$ channel, partly moving through this channel, and reflected back into the entrance channel, respectively. For $L=30$ and 40, the two actions of the stretch and breakaway can be seen clearly. However, only the stretch motion is present for $L=50$.

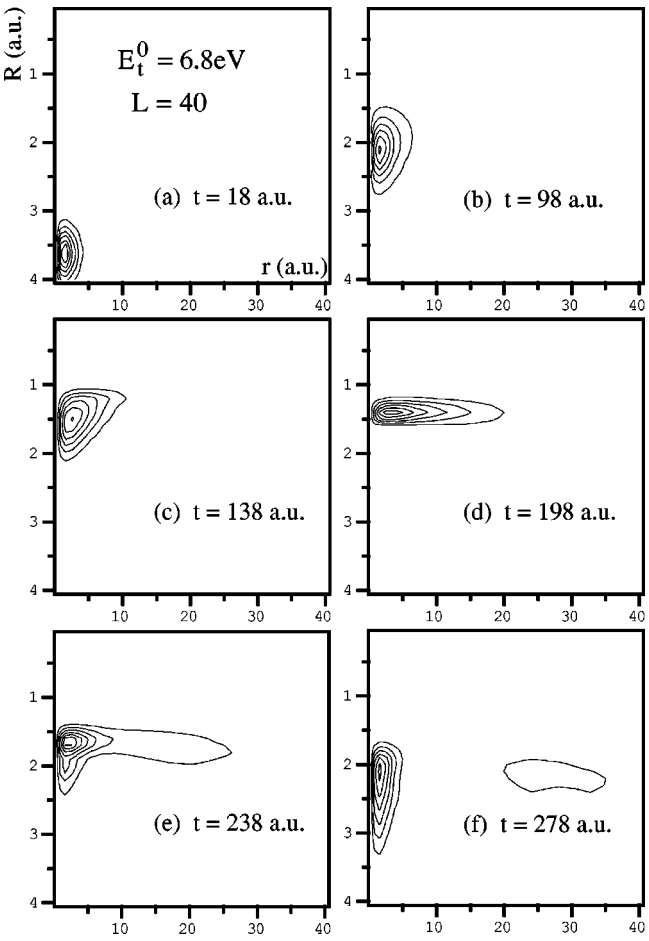

FIG. 3. Plots of the probability distribution $\rho^{L=40}(R,r,t)$ for $E_t^0=6.8$ eV at different points of time, as shown by contours.

We also display in Fig. 4 the electron distribution calculated by using the SC method of paper I. The SC electron distribution may be defined in the same way as Eq. (3.1) except for the radial distance R. In the SC calculation, the translational energy E_t and the initial distance R have been set to be equal to the corresponding central values of the wave packet (i.e., E_t^0 and R^0). It should be noted that the initial wave packet spans some range of E_t or R, which depends on the width parameter δ through Eq. (2.18). Hence, the QM electron distribution reflects the overlapping for various energies or various initial distances. In this sense, we may not have to make a detailed comparison between the QM and SC results. Nevertheless, the comparison is very interesting, and we see a close similarity between the QM and SC electron distributions in Fig. 4. From this result, we may expect that the SC method is very useful to describe the QM motion of the electron during the collision.

For the cases shown in Fig. 4, we have further calculated the time dependence of the average radial distances,

$$\langle R(t)\rangle = \int R\rho^L(R,r,t)dRdr, \tag{3.3}$$

$$\langle r(t)\rangle = \int r\rho^L(R,r,t)dRdr. \tag{3.4}$$

The results are shown in Fig. 5. The smallest value of $\langle R(t)\rangle$ will be helpful to characterize the reflection position in the wave-packet propagation. The average distance $\langle r(t)\rangle$ may measure the extent of the electron cloud. When $L=30$ and 40, as seen in Fig. 4, the wave packet has a finite amplitude at large r. However, once a portion of the wave packet reaches $r>r_{op}$, that will be absorbed by the imaginary potential. For this reason, tracing the time evolution of the average distances has no meaning after the absorption of the wave packet begins. Therefore, the curves are drawn only for the time range that the absorption is negligible.

In Fig. 5, we also show the time dependence of the average distances calculated by the SC method of paper I. We can see that the average distance $\langle r(t)\rangle$ is nicely described by the SC method as expected from Fig. 4. The average value $\langle R(t)\rangle$ is also very close to the SC quantity $R_{sc}(t)$, which is just given by a common trajectory itself. The usefulness of the SC method for predicting the average distances is easily understandable in the cases of $L=30$ and 50 because most of the collisions induce merely single process (elastic transition or protonium formation). When $L=40$, as may be seen in Fig. 4, however both the elastic and protonium formation processes will occur equally in the collisions. Hence, in the classical treatment, two quite different kinds of trajectories (i.e., recoil and capture) must be considered for the $\bar{p}$ motion at the same time. The common trajectory assumption would be no more valid in such case. Nevertheless, we find in Fig. 5 that the common trajectory $R_{sc}(t)$ is still a good approximation to $\langle R(t)\rangle$ even for $L=40$.

B. Formation probabilities

First, we compare the formation probabilities calculated by the present QM method with the SC results of paper I at three energies $E_t=4.0$, 6.8, and 10.0 eV. In Fig. 6, we show the opacities defined by $(2L+1)P_{pp}^L$ as a function of the total angular momentum L. From Eq. (2.25), the summation of the opacities over L provides the quantity proportional to the formation cross section. The SC opacities are found to be very close to the QM ones for L higher than and also much lower than the peak position. However, around the peak, the SC calculation gives larger opacities, and even exhibits peculiar L dependence.

To understand the L dependence of the SC formation probabilities, it may be helpful to consider the energy conservation expected to be satisfied in the SC calculation, i.e.,

$$E_t - I_{1s} = E_t' + \epsilon P_{sc}^L - I_{1s}(1-P_{sc}^L), \tag{3.5}$$

where E_t' is the final translational energy, ϵ is the mean energy loss due to the electron emission, and P_{sc}^L is the SC probability for the electron emission. In the common trajectory treatment, it may be judged that the antiproton is certainly captured if $E_t'<0$. Since $\epsilon>0$, we find that the condition $E_t'<0$ holds whenever the emission probabilities are $P_{sc}^L>E_t/I_{1s}$. (It should be noted, however, that there is no definite way to evaluate the emission probability in the common trajectory treatment when $P_{sc}^L>E_t/I_{1s}$.) Consequently, the SC formation probabilities become unity for P_{sc}^L

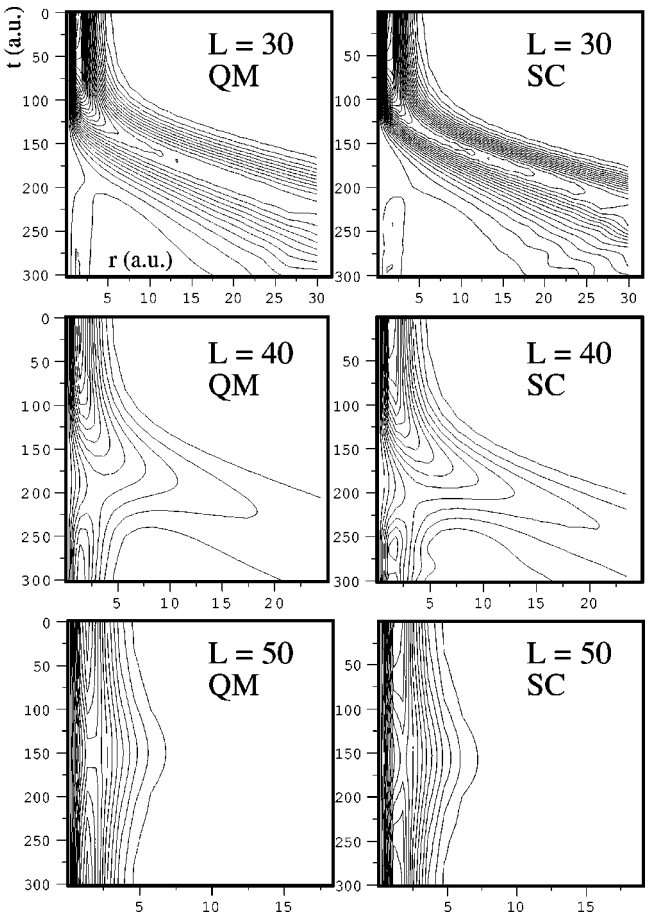

FIG. 4. Time evolution of the electron distribution $\rho^{L=30,40,50}(r,t)$, as shown by contours. The QM and SC results are for $E_t^0=7.5$ eV and $E_t=7.5$ eV, respectively.

$>E_t/I_{1s}$. This appears in Fig. 6 as a linear curve ($=2L+1$) of the SC results from $L=0$ to the critical peak position L_c defined by $P_{sc}^{L_c}\simeq E_t/I_{1s}$.

When $L>L_c$, the common trajectory exhibits a behavior of only the recoil motion for the antiproton although the capture is possible in the QM calculation unless L is much higher than L_c. (Accordingly, the SC emission probability P_{sc}^L could be rather evaluated in paper I.) It has been assumed in paper I that the formation probability is given by $P_{\bar{p}p}^L=P_{sc}^L$ for $L>L_c$. From Fig. 6, we see that this assumption is acceptable. It is very interesting that the SC method, which offers only a recoil behavior of the common trajectory, is still useful to describe the protonium formation. As may be seen in Fig. 3 (or shown in paper I), the electron is ejected rapidly only around the reflection position (i.e., the first turning point). Hence, the common trajectory would not deviate so much from real trajectories at least until it reaches the first turning point, and consequently, we could calculate the emission probability for $L>L_c$ in a reasonable accuracy by using the common trajectory. We can see in Fig. 5 that the common trajectory is in fact a good approximation to $\langle R(t)\rangle$. When $L>L_c$, it should be noted that although the common trajectory treatment will be justified for the calculation of the formation probability summed over all the final states, it can never provide any information on the bound motion of the protonium atom.

In the QM calculation, the formation probabilities $P_{\bar{p}p}^L$ are close to, but not equal to unity for $L\ll L_c$. Hence, the SC probabilities are slightly larger than the QM ones there. The error of the SC probability becomes the largest $\sim 100\times(1-E_t/I_{1s})\%$ at $L=L_c$. As a result, the main error of the SC calculation for the cross section comes from L's equal to and slightly lower than L_c. If we may evaluate the emission probabilities P_{sc}^L for the low $L(\leqslant L_c)$, the SC method will give more reliable formation probabilities by equating $P_{\bar{p}p}^L=P_{sc}^L$.

In paper I, we have found that the position of the first turning point of the common trajectory is a key point to understand the mechanism of the electron emission, and furthermore that the turning point may be well estimated from the adiabatic potential. Accordingly, we show in Fig. 7 the present QM formation probabilities as plotted against the turning point R_{tp}^{ad} for the adiabatic potential. The probabilities are displayed in the same figure for the translational energies $E_t=3.5$, 5.0, 6.8, and 10.0 eV all together. A very interesting thing is that all the points are almost put on a single curve. This result supports the finding of paper I that the relative motion of $\bar{p}$ and H can be nicely described by the adiabatic potential at least until reaching the first turning point. We may further expect that the turning point is the almost only important factor to determine the dynamics of the protonium formation (1.1) in the present energy region.

The solid line in Fig. 7 is a fit of all the data for $E_t=2.72$–10 eV, and its function form is assumed as

$$P_{fit}(R_{tp}^{ad})=\frac{a}{b+R_{tp}^{ad}}\exp[-c(R_{tp}^{ad}-d)^4], \tag{3.6}$$

where $R_{tp}^{ad}<2$ a.u. and $a=88$, $b=94.5$, $c=2.3$, $d=0.426$. For $R_{tp}^{ad}\lesssim R_{FT}$ (except very small R_{tp}^{ad}), the probabilities take a nearly constant value $P_c\simeq 0.93$. By using this fit, we may calculate the formation probabilities for any energies where the calculation has not been made. For the adiabatic turning points R_{tp}^{ad} ranging from $\sim R_{FT}$ to 2 a.u., the formation probability decreases to zero, but has a significant contribution to the cross section. This fact indicates the importance of nonadiabatic coupling for the low-energy formation process (1.1).

C. Formation cross sections

In Fig. 8, we plot the formation cross sections $\sigma_{\bar{p}p}^-$ as a function of the translational energy E_t. The present QM cross section is compared with those calculated by the SC method (paper I), the CTMC method [4], the CTMC method with the pseudopotential [4], and the adiabatic method [8]. The adiabatic cross section is given by assuming that the formation probability is unity if $R_{tp}^{ad}\leqslant R_{FT}$ and is otherwise zero. The usefulness of the adiabatic potential mentioned above appears as the fact that the energy dependence of the adiabatic cross section is similar to the QM one. However, the adiabatic method significantly underestimates the formation cross section at these energies as found in paper I. The

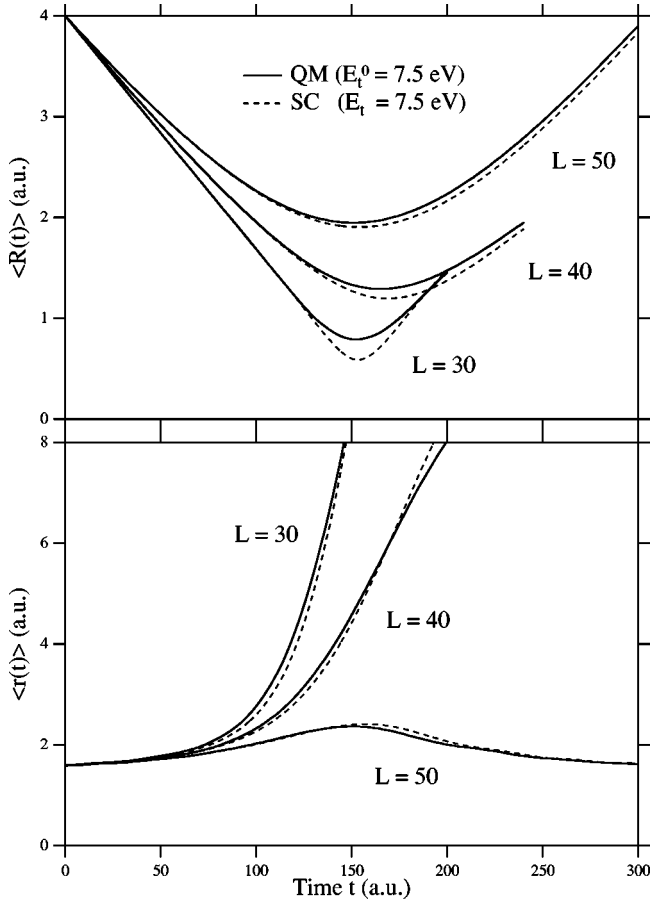

FIG. 5. Time dependence of the average distances $\langle R(t)\rangle$ and $\langle r(t)\rangle$ for $L=30$, 40, and 50. The QM and SC results are for $E_t^0=7.5$ eV and $E_t=7.5$ eV, respectively. On the upper panel, the common trajectory $R_{sc}(t)$ is shown for the SC results.

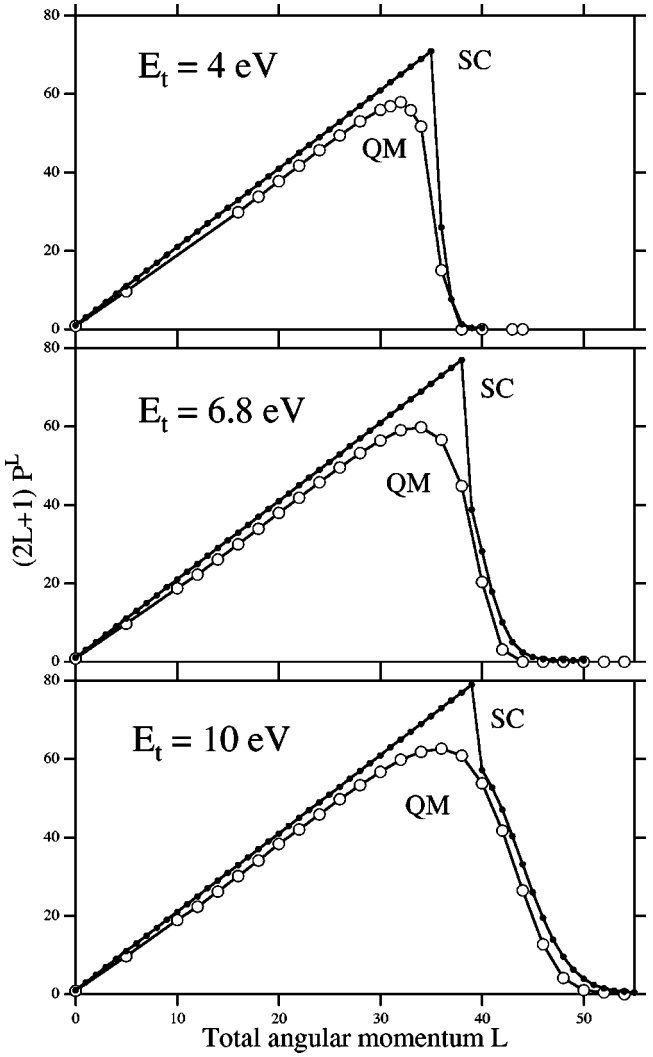

FIG. 6. Opacities $(2L+1)P_{pp}^{L}$ as a function of the total angular momentum L for $E_t=4.0$, 6.8, and 10.0 eV. The SC results of paper I are also shown.

SC cross sections are about 15% larger than the QM ones. As seen in Fig. 6, this error manly comes from the defect of the common trajectory treatment for $L\leqslant L_c$. The CTMC cross sections are larger than the QM results for the high energies and smaller for the low energies. When the pseudopotential is introduced to present a QM effect in the CTMC calculation, the cross section becomes much closer to the QM value. This result suggests that the QM nature is important in the protonium formation (1.1).

D. Angular momentum distribution of protonium

In the CTMC study, Cohen [4] calculated the level distribution of the protonium atom formed in the process (1.1). Since we have not made a complete analysis of the wave packet for the arrangement channel $e+\bar{p}p$, we cannot obtain the accurate level distribution of the protonium atom. Nevertheless, since very high total angular momenta ($L\gg l$) are mostly important in the protonium formation (1.1), it would be allowed that the angular momentum $\bar{l}$ of the protonium atom is approximated by $\bar{l}=L$. (See, also, the Appendix.) Therefore, we may define the relative fraction of the protonium atom having the angular momentum $\bar{l}$ as

$$f(\bar{l})=\frac{(2\bar{l}+1)P_{pp}^{L=\bar{l}}}{\sum_L (2L+1)P_{pp}^{L}}. \tag{3.7}$$

In Fig. 9, the relative fractions calculated in this way are shown for three energies $E_t=2.72$, 5.44, and 8.16 eV, and are compared with the analytical fits of the CTMC results given by Cohen [4]. In contrast to the case of the cross section, it seems that the relative fraction given by the pure CTMC method (without the pseudopotential) agrees rather better with the QM result.

IV. SUMMARY AND FURTHER DISCUSSION

We have applied a time-dependent full QM wave-packet propagation method to a Coulomb three-body ($\bar{p}$+H) collision problem. A DVR technique has been employed for the numerical calculation. Cross sections have been obtained for the protonium formation process $\bar{p}+\mathrm{H}\rightarrow\bar{p}p+e$ at transla-

tional energies below 10 eV. Although the time-dependent full QM approach has been widely accepted in the field of chemical reaction [21,23,28], the present work is probably its first application to heavy particle collisions of the atomic Coulomb system. The present study and recent application to the electron-impact ionization vigorously made by Pindzola and Schultz, and Robicheaux, and Colgan *et al.* [30] encourage the theoretical treatment based on the time-dependent picture also in atomic collision processes.

A plot of the QM formation probabilities $P_{\bar{p}p}^{L}$ for various energies against the adiabatic turning points $R_{\rm tp}^{\rm ad}$ gives a universal curve in a good approximation. The adiabatic potential and especially the adiabatic turning point are of critical importance to understanding the mechanism of the protonium formation. However, it does not mean that the adiabatic picture is fully acceptable. The significance of the adiabatic turning points $R_{\rm tp}^{\rm ad} > R_{\rm FT}$ for the protonium formation indicates that the nonadiabatic transition is very important in this process.

Paper I has shown that when the translational energy is below 1.57 eV, the formation cross section is identical to the so-called orbiting cross section $\sigma_{\rm orb}^{\rm ad}$ that is obtained using the adiabatic potential. It is not easy to extend the present calculation to these low energies because the wave-packet propagation must be performed for a very long time. Nevertheless, the present results may be helpful to estimate the formation cross section in the orbiting energy region. We have found that the protonium formation occurs in the probability of $P_{\rm c}$ ($\simeq 0.93$) in cases of $R_{\rm tp}^{\rm ad} \lesssim R_{\rm FT}$. Paper I has suggested that when L is lower than the critical value that the orbiting occurs, the relative motion to the small distances $R \lesssim R_{\rm FT}$ becomes classically allowed. Therefore, we may expect that the formation cross section in the orbiting energy region is given by $\sigma_{\bar{p}p}^{-} = P_{\rm c}\sigma_{\rm orb}^{\rm ad}$, which is about 10% smaller than the orbiting value. It should be noted that the orbiting approach becomes meaningless at extremely low energies since it is a classical picture. In fact, the orbiting treatment gives too large cross sections at energies of $E_{\rm t} < 10^{-6}$ eV [11].

It has been shown that the SC method assuming a common trajectory [10] can describe well the time evolution of some QM quantities. Therefore, the SC method is very useful to gain a physical understanding of the collision dynamics in $\bar{p}$+H. However, the SC method is not always reliable to obtain an accurate formation probability just because the common trajectory is assumed. It is very interesting to invent a more sophisticated trajectory for the relative motion in the SC method.

In a CTMC method [4], if a pseudopotential is added in the interaction, the formation cross section agrees well with the QM results at the energies considered in the present study. For relative angular momentum distribution, the pure CTMC method (without the pseudopotential) [4] seems to be rather better. It should be noted, however, that the CTMC methods both with and without the pseudopotential [4] give the formation cross sections (respectively, 163 and 67 a.u.) largely different from the orbiting value $\sigma_{\rm orb}^{\rm ad}$ (=91 a.u.) at $E_{\rm t} = 0.272$ eV.

It would be interesting to compare the present results with those of the QM study of Voronin and Carbonell [11]. However, unfortunately, the time-dependent picture is not appropriate for the calculation of the collisions at extremely low energies because of the necessity of very-long-time propagation and still more the diffuseness of the wave packet. The time-independent picture will be much more suitable for extremely low energies.

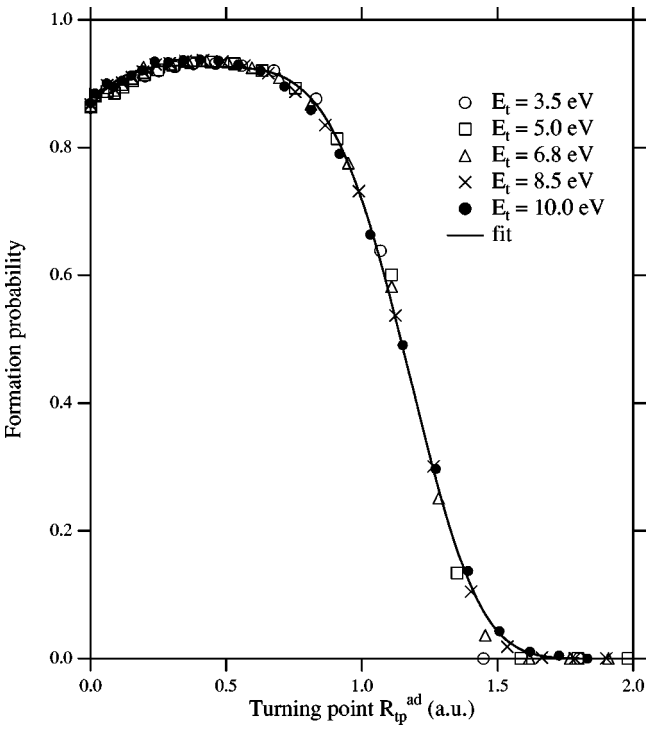

FIG. 7. Formation probabilities $P_{\bar{p}p}^{L}$ are plotted against the adiabatic turning points $R_{\rm tp}^{\rm ad}$ for $E_{\rm t} = 3.5$, 5.0, 6.8, and 10.0 eV. A solid curve is a fit of all the data for $E = 2.72$–10.0 eV.

It is very important to obtain the final-state specified cross sections for the protonium formation. To calculate the accurate cross sections specified by the principal and angular momentum quantum numbers $(\bar{n},\bar{l})$ of the protonium atom, the coordinates $(\mathbf{R},\mathbf{r})$ must be transformed into another set of Jacobi coordinates $(\mathbf{Q},\mathbf{q})$, which correspond to the arrangement channel $e+\bar{p}p$. (See the Appendix.) In doing an analysis of the final wave packet, we must remember that the Laguerre grid is not appropriate because the grid points become scattered for large distances. To avoid this problem, for instance, we will be able to take the following step: the wave packet is propagated using the present numerical method until it reaches a reaction zone, the transformation $(\mathbf{R},\mathbf{r}) \rightarrow (\mathbf{Q},\mathbf{q})$ is made there, the Chebyshev grid is applied both for the $\mathbf{Q}$ and $\mathbf{q}$ coordinates, and then the wave packet may be propagated into sufficiently large q. The calculation of the final-state specified cross sections for the protonium formation remains in future work.

When the translational energy is higher than the ionization energy (=13.6 eV) of the hydrogen atom, the breakup ionization $\bar{p}+p+e$ becomes an open channel. The CTMC studies [6,4] showed that the protonium formation (1.1) was negligible at $E_{\rm t} > 15$ eV. Of special interest is the question

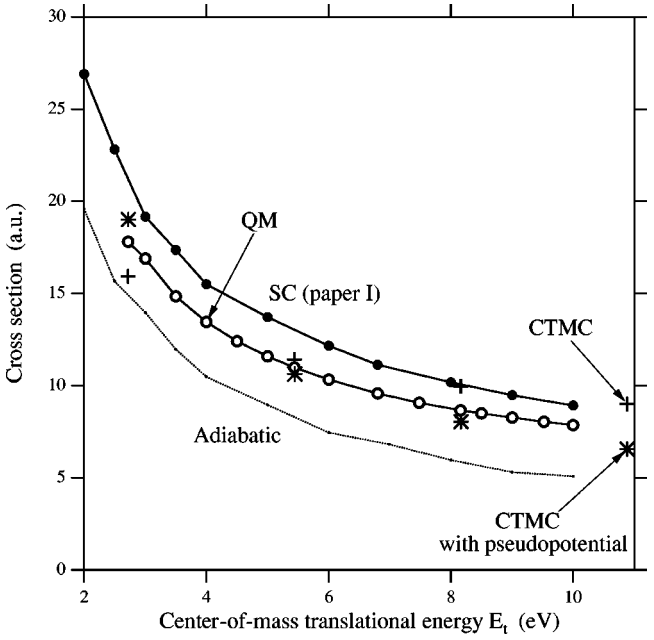

FIG. 8. Formation cross sections $\sigma_{p\bar{p}}$ as a function of the translational energy E_t. The SC results are taken from paper I. The results of the CTMC method and the one with the pseudopotential are given by Cohen [4]. The cross sections obtained under the adiabatic assumption are also shown.

whether the SC method with the common trajectory assumption is satisfactory also to describe the breakup ionization. The extension of the present QM approach to the energy region above the ionization threshold may be made straightforwardly. The full QM calculation for the breakup ionization and the comparison with the SC results will be reported in a next study [31].

ACKNOWLEDGMENTS

This research was partially supported by the Grant-in-Aid for Scientific Research on Priority Areas ''Molecular Physical Chemistry'' from the Ministry of Education, Culture, Sports, Science and Technology.

APPENDIX: ASYMPTOTIC FORM FOR PROTONIUM FORMATION

For the arrangement channel $e+\bar{p}p$, we have a set of Jacobi coordinates **Q** and **q**, which are the position vectors of $\bar{p}$ from p and of e from the center-of-mass of $\bar{p}p$, respectively. The coordinates **Q** and **q** are expressed in terms of **R** and **r** as

$$\mathbf{Q}=\mathbf{R}+\frac{m_e}{m_e+m_p}\mathbf{r}, \quad \mathbf{q}=-\frac{1}{2}\mathbf{R}+\frac{m_e+2m_p}{2(m_e+m_p)}\mathbf{r}. \quad \text{(A1)}$$

Because $m_e \ll m_p$, we may set $\mathbf{Q}=\mathbf{R}$ unless r is too large. Therefore, in the BF frame ($\hat{z}=\hat{\mathbf{R}}$), the time-independent wave function (2.10) may be re-expressed as

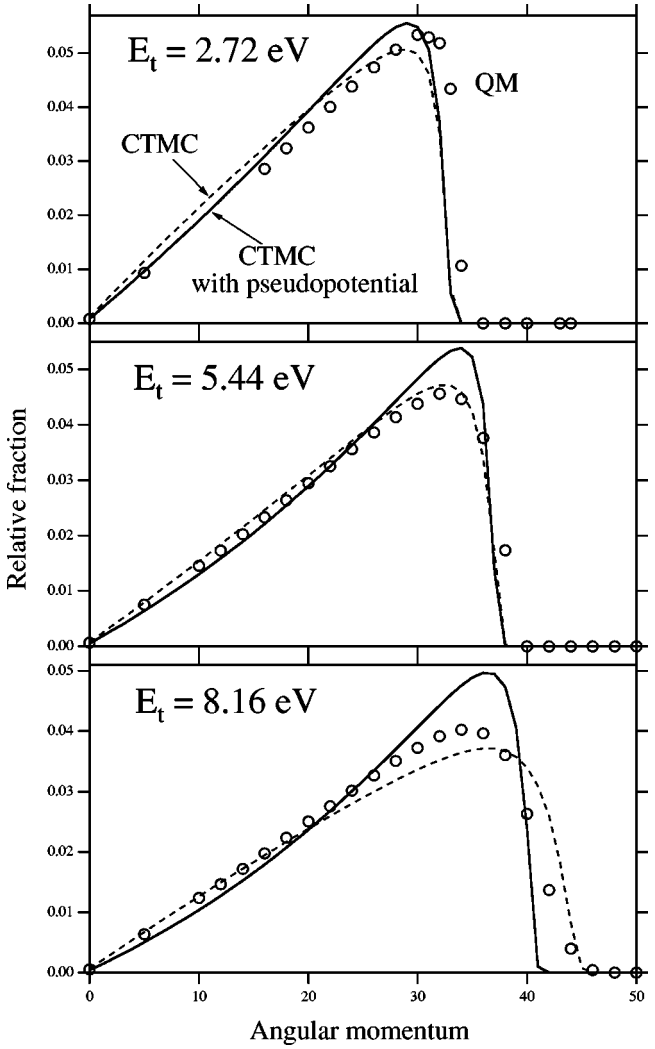

FIG. 9. Relative angular momentum distribution of the protonium atom $f(\bar{l})$ for $E_t=2.72$, 5.44, and 8.16 eV. The results of the CTMC method and the one with the pseudopotential are taken from Cohen [4].

$$\Psi^{LM}(E)=(Rq)^{-1}\sum_{\lambda}\bar{D}^{L}_{M\lambda}(\alpha,\beta,\gamma')\psi^{L\lambda}(R,q,\phi,E), \quad \text{(A2)}$$

where $\hat{\mathbf{q}}=(\phi,\gamma')$.

For sufficiently large q, the wave-function $\psi^{L\lambda}(R,q,\phi,E)$ becomes

$$\psi^{L\lambda}(R,q,\phi,E)=-\sum_{nl\lambda'}\bar{P}^{\lambda}_{l}(\cos\phi)\,\eta^{L\bar{n}l}_{\lambda,\lambda'}(R)\sqrt{\frac{m'}{2\pi k^{-}_{n}}} \times\exp(+\mathrm{i}\,k^{-}_{n}q)S^{L}_{\bar{n}l\lambda',\Gamma_0\lambda_0}, \quad \text{(A3)}$$

where $\bar{P}^{\lambda}_{l}$ is the normalized associated Legendre function, l is the electronic angular momentum quantum number, m' is the reduces mass of the $e+\bar{p}p$ system, k^{-}_{n} is the wave number of the ejected electron, and $S^{L}_{\bar{n}l\lambda',\Gamma_0\lambda_0}$ is the S-matrix

element for the protonium formation. In Eq. (A3), the radial wave function of the protonium $\eta^{L\bar{n}\bar{l}}_{\lambda,\lambda'}(R)$ in the BF frame is defined by

$$\eta^{L\bar{n}\bar{l}}_{\lambda,\lambda'}(R)=\sum_{l}\frac{2\bar{l}+1}{2L+1}(\bar{l}0l\lambda|L\lambda)\,\eta_{\bar{n}\bar{l}}(R)(\bar{l}0l\lambda'|L\lambda'), \tag{A4}$$

where $\eta_{\bar{n}\bar{l}}(R)$ is the ordinary radial Coulomb function, and $(\bar{n},\bar{l})$ are the quantum numbers of the protonium atom. It should be noted, however, that the final magnetic component λ' in $S^{L}_{\bar{n}l\lambda',\Gamma_0\lambda_0}$ is not a good quantum number even in the limit of $q\to\infty$. If we describe the protonium state in the SF frame, the *S*-matrix element becomes

$$S^{L}_{\bar{n}\bar{l}l,\Gamma_0\lambda_0}=\sum_{\lambda'}\left(\frac{2\bar{l}+1}{2L+1}\right)^{1/2}(\bar{l}0l\lambda'|L\lambda')S^{L}_{\bar{n}l\lambda',\Gamma_0\lambda_0}. \tag{A5}$$

Since the electronic angular momentum l is very small compared with L in most cases, we may assume $\bar{l}=L$ in Eq. (A4). Then, we have

$$\eta^{L\bar{n}\bar{l}}_{\lambda,\lambda'}(R)=\eta_{\bar{n}L}(R)\,\delta_{\lambda\lambda'}, \tag{A6}$$

and the asymptotic form of $\psi^{L\lambda}(E)$ becomes

$$\psi^{L\lambda}(R,q,\phi,E)=-\sum_{\bar{n}l}\bar{P}^{\lambda}_{l}(\cos\phi)\,\eta_{\bar{n}L}(R)\sqrt{\frac{m'}{2\pi k_{\bar{n}}}}\times\exp(+\mathrm{i}\,k_{\bar{n}}q)S^{L}_{\bar{n}l\lambda,\Gamma_0\lambda_0}. \tag{A7}$$

This approximation is just the same as the one usually done in the study of molecular spectroscopy: i.e., the Coriolis coupling is neglected for the $\bar{p}$-p motion in the BF (rotating protonium) frame.

[1] J. Eades and F. J. Hartmann, Rev. Mod. Phys. **71**, 373 (1999).
[2] M. H. Holzscheiter and M. Charlton, Rep. Prog. Phys. **62**, 1 (1999).
[3] J. S. Cohen, Phys. Rev. A **36**, 2024 (1987).
[4] J. S. Cohen, Phys. Rev. A **56**, 3583 (1997).
[5] J. S. Cohen, Phys. Rev. A **59**, 1160 (1999).
[6] D. R. Schultz, P. S. Krstić, C. O. Reinhold, and J. C. Wells, Phys. Rev. Lett. **76**, 2882 (1996).
[7] C. L. Kirschbaum and L. Wilets, Phys. Rev. A **21**, 834 (1980).
[8] D. L. Morgan, Jr. and V. W. Hughes, Phys. Rev. A **2**, 1389 (1970); **7**, 1811 (1973).
[9] D. L. Morgan, Jr., in *International School of Physics of Exotic Atoms, 6th Workshop: Exotic Atoms, Molecules and Their Interactions*, edited by C. Rizzo and E. Zavattini (Servizio di Riproduzione della Sezione dell'INFN di Trieste, Trieste, 1994), p. 205.
[10] K. Sakimoto, J. Phys. B **34**, 1769 (2001).
[11] A. Y. Voronin and J. Carbonell, Phys. Rev. A **57**, 4335 (1998).
[12] N. H. Kwong, J. D. Garcia, and J. S. Cohen, J. Phys. B **22**, L633 (1989).
[13] J. C. Light, I. P. Hamilton, and J. V. Lill, J. Chem. Phys. **82**, 1400 (1985); D. Baye and P. H. Heenen, J. Phys. A **19**, 2041 (1986).
[14] K. Sakimoto, J. Phys. B **33**, 3149 (2000).
[15] K. Sakimoto, J. Phys. B **33**, 5165 (2000).
[16] R. T. Pack, J. Chem. Phys. **60**, 633 (1974).
[17] J. M. Launay, J. Phys. B **9**, 1823 (1976).
[18] E. B. Wilson and J. B. Howard, J. Chem. Phys. **4**, 260 (1936).
[19] M. E. Rose, *Elementary Theory of Angular Momentum* (Willey, New York, 1957).
[20] R. Walls, R. Herman, and H. W. Milnes, J. Mol. Spectrosc. **4**, 51 (1960).
[21] M. H. Beck, A. Jäckle, G. A. Worth, and H.-D. Meyer, Phys. Rep. **324**, 1 (2000).
[22] D. E. Manolopoulos and M. H. Alexander, J. Chem. Phys. **97**, 2527 (1992).
[23] G. Nyman and H.-G. Yu, Rep. Prog. Phys. **63**, 1001 (2000).
[24] F. Calogero, J. Math. Phys. **22**, 919 (1981); J. T. Muckerman, Chem. Phys. Lett. **173**, 200 (1990).
[25] *Handbook of Mathematical Functions*, Natl. Bur. Stand. Appl. Math. Ser., edited by M. Abramowitz and I. A. Stegun (U.S. GPO, Washington, D.C., 1964), p. 773.
[26] K. Sakimoto, Chem. Phys. **249**, 1 (1999); J. Chem. Phys. **112**, 5044 (2000).
[27] M. J. Bramley and N. C. Handy, J. Chem. Phys. **98**, 1378 (1993).
[28] B. Balakrishnan, C. Kalyanararnan, and N. Sathyamurthy, Phys. Rep. **280**, 79 (1997).
[29] D. Neuhauser, M. Baer, R. S. Judson, and D. J. Kouri, J. Chem. Phys. **90**, 5882 (1989).
[30] M. S. Pindzola and D. R. Schultz, Phys. Rev. A **53**, 1525 (1996); M. S. Pindzola and F. Robicheaux, *ibid.* **57**, 318 (1998); J. Colgan, M. S. Pindzola, D. M. Mitnik, and D. C. Griffin, *ibid.* **63**, 062709 (2001); and references therein.
[31] K. Sakimoto (unpublished).